Astronomy & Astrophysics

Suzaku observation of the LINER NGC 4102

O. González-Martín[1,2], I. Papadakis[1,2], V. Braito[3], J. Masegosa[4], I. Márquez[4], S. Mateos[3], J. A. Acosta-Pulido[5,6], M. A. Martínez[4,7], J. Ebrero[8], P. Esquej[3], P. O'Brien[3], J. Tueller[9], R. S. Warwick[3], and M. G. Watson[3]

[1] IESL, Foundation for Research and Technology, 711 10 Heraklion, Crete, Greece
   e-mail: omaira@physics.uoc.gr; omaira@physics.uoc.gr
[2] Physics Department, University of Crete, PO Box 2208, 710 03 Heraklion, Crete, Greece
[3] Department of Physics and Astronomy, Leicester University, LE1 7RH, UK
[4] Instituto de Astrofísica de Andalucía (CSIC), Granada, Spain
[5] Instituto de Astrofísica de Canarias (IAC), C/Via Lactea, s/n, 38205 La Laguna, Tenerife, Spain
[6] Departamento de Astrofísica, Universidad de La Laguna, 38205 La Laguna, Tenerife, Spain
[7] Grupo de Mecánica Espacial and Instituto Universitario de Matemática y Aplicaciones, Universidad de Zaragoza, 50009 Zaragoza, Spain
[8] SRON Netherlands Institute for Space Research, Sorbonnelaan 2, 3584 CA, Utrecht, The Netherlands
[9] NASA Goddard Space Flight Center, Astrophysics Science Division, Greenbelt, MD 20771, USA

ABSTRACT

Context. Low-ionisation, nuclear emission-line region (LINER) nuclei are said to be different from other active galactic nuclei (AGN) due to the presence of complex absorbing structures along the line-of-sight and/or an inefficient mode of accretion onto the supermassive black hole. However, this is still open.
Aims. We investigate the broad band X-ray spectrum of NGC 4102, one of the most luminous LINERs in the Swift/BAT survey.
Methods. We studied a 80 ks *Suzaku* spectrum of NGC 4102, together with archival *Chandra* and Swift/BAT observations. We also studied the optical (3.5 m/TWIN at Calar Alto observatory) and near-infrared (WHT/LIRIS at Observatorio Roque los Muchachos) spectra that were taken at the same time as the *Suzaku* data.
Results. There is strong evidence that NGC 4102 is a *Compton*-thick AGN, as suggested by the Swift/BAT detected intrinsic continuum and the presence of a strong narrow, neutral FeKα emission line. We have also detected ionised Fe$_{XXV}$ emission lines in the *Suzaku* spectrum of the source. NGC 4102 shows a variable soft excess found at a significantly higher flux state at the time of *Suzaku* observations when compared to *Chandra* observations. Finally, a complex structure of absorbers is seen with at least two absorbers besides the *Compton*-thick one, derived from the X-ray spectral analysis and the optical extinction.
Conclusions. All the signatures described in this paper strongly suggest that NGC 4102 is a *Compton*-thick Type-2 AGN from the X-ray point of view. The "soft excess", the electron scattered continuum component, and the ionised iron emission line might arise from *Compton*-thin material photoionised by the AGN. From variability and geometrical arguments, this material should be located somewhere between 0.4 and 2 pc away from the nuclear source, inside the torus and perpendicular to the disc. The bolometric luminosity ($L_{bol} = 1.4 \times 10^{43}$ erg s^{-1}) and accretion rate ($\dot{m}_{Edd} = 5.4 \times 10^{-3}$) are consistent with other low-luminosity AGN. However, the optical and near infrared spectra correspond to that of a LINER source. We suggest that the LINER classification might be due a different spectral energy distribution according to its steeper spectral index.

Key words. galaxies: active – galaxies: nuclei – galaxies: Seyfert – galaxies: individual: NGC 4102 – X-ray: galaxies

1. Introduction

Active galactic nuclei (AGN) emit over the entire electromagnetic spectrum and are widely believed to be powered by the accretion of matter onto a supermassive black hole (SMBH, Rees 1984). Several families within the AGN category have been established from observations. Although their classification is sometimes misleading, a unified model is proposed to explain them all under a single scenario (Antonucci 1993). A key ingredient in this scheme is a dusty torus whose inclination with respect to the observer's line of sight is responsible for the dichotomy between optical Type-1 (with broad permitted lines, face-on view) and Type-2 (with narrow permitted lines, edge-on view) AGN. However, this scheme needs to be refined further since there are several sub-classes of objects that cannot be easily fitted into this scenario (for example unobscured Type 2 Seyferts, e.g. Mateos et al. 2005; Dewangan & Griffiths 2005; Panessa & Bassani 2002).

One of the most intriguing cases are low-ionisation, nuclear emission-line regions (LINERs, Heckman 1980). As suggested by their low X-ray luminosities ($L(2–10$ keV) $\sim 10^{39–42}$ erg s^{-1}, see González-Martín et al. 2009a), they could be the link between AGN ($L(2–10$ keV) $\sim 10^{41–45}$ erg s^{-1}) and normal galaxies ($\sim 10^{38–42}$ erg s^{-1}, Fabbiano 1989). Moreover, they are the dominant population of active galaxies in the nearby universe (Ho et al. 1997). However, their nature has not yet been well understood.

Several samples of LINERs have been analysed at X-ray frequencies, a large fraction of them showing AGN signatures (González-Martín et al. 2009a; González-Martín et al. 2006; Dudik et al. 2005). In spite of this, it still remains unclear how to fit LINERs into the AGN unification scenario. A radiatively

inefficient accretion flow onto the SMBH (Ho 2009) and/or the presence of highly obscuring matter have been proposed to explain the differences between LINERs and more luminous AGN (Goulding & Alexander 2009; Dudik et al. 2009; González-Martín et al. 2009b).

Using the ratio $\log(F\mathrm{x}(2\text{–}10\ \mathrm{keV})/F([\mathrm{O\ III}]))$ ($R_{\mathrm{X/[O\ III]}}$, hereinafter), González-Martín et al. (2009b) showed that LINERs have more *Compton*-thick sources than Type-2 Seyfert galaxies. This implies high column densities and significant suppression of the intrinsic continuum emission below 10 keV. Only indirect proof of their Compton-thickness can be obtained with *Chandra* and *XMM-Newton* data. Therefore, the nature of these sources still needs to be confirmed. More direct evidence comes from the determination of the strength of the neutral iron Kα emission line and the direct view of the nuclear continuum above 10 keV.

NGC 4102 is a nearby Sb galaxy with a nuclear optical spectrum that was first classified as an HII region by Ho et al. (1997) although its UV emission is not compatible with this classification (Kinney et al. 1993). Gonçalves et al. (1999) classified its optical spectrum as composite, concluding that the nucleus is dominated by starburst emission, although a weak Type-2 Seyfert component is also present. NGC 4102 is included in the Carrillo et al. (1999) sample of LINERs[1], and we have reclassified it as LINER by means of the emission lines given in Moustakas & Kennicutt (2006).

NGC 4102 has been observed with the *Chandra*/ACIS snapshot survey (Dudik et al. 2005). They classify it as an AGN-like source. Tzanavaris & Georgantopoulos (2007) point out its AGN signatures, and consider it as a good candidate for harbouring a hidden AGN. They claim there is an iron line, although poor statistics do not allow them to accurately constrain its equivalent width. Ghosh et al. (2008) show that NGC 4102 has an AGN and strong star formation activity. They also point out the existence of a reflection component based on a hint of a strong FeKα emission line. According to the $F_{\mathrm{X}}(2\text{–}10\ \mathrm{keV})/F([\mathrm{O\ III}])$ ratio, NGC 4102 is a good candidate to be a *Compton*-thick source (see Sect. 5 in this paper). Therefore, NGC 4102 is an ideal case for studying the obscuration in LINERs.

Here we present the *Suzaku* spectra of NGC 4102. We also present optical (TWIN/2.2 m in Calar Alto observatory) and near infrared (LIRIS/WHT in El Roque de los Muchachos observatory) spectra, which were taken contemporaneously (up to one month apart) with our *Suzaku* observation. *Chandra* archival data are also revisited to study the long-term variability of this source.

This paper is organised as follows. In Sect. 2 we describe the X-ray data reduction and observations. In Sect. 3 we present the X-ray spectral fitting. In Sect. 4 we review the NGC 4102 activity classification as seen by optical and near-IR observations. Finally, we discuss the nature of the emission seen in NGC 4102 in Sect. 5 and report the main conclusions in Sect. 6. A distance of 17 Mpc is assumed for NGC 4102 throughout the analysis (Tully 1988), as is ΛCDM cosmology with $(\Omega_{\mathrm{M}}, \Omega_{\Lambda}) = (0.3, 0.7)$ and $H_0 = 75$ km s^{-1} Mpc^{-1} (i.e. $z = 0.0042$).

2. X-ray observations and data reduction

2.1. Suzaku data

Suzaku (Mitsuda et al. 2007) observed NGC 4102 for a total exposure time of 80 ks on 2009 May 30. The data were taken using the X-ray Imaging Spectrometer (XIS) and the Hard X-ray Detector (HXD) at the HXD nominal point[2]. For the data reduction and analysis we followed the latest *Suzaku* data reduction guide[3]. We reprocessed all the data files using standard screening within XSELECT ("SAA==0" and "ELV > 5").

The net exposure time of XIS detectors is 79 ks. We reprocessed the spaced-row charge injection (CTI) data of the XIS instrument using XISPI task in order to use the latest calibration files at the time of writing. We also excluded data with Earth day-time elevation angles below 20° using XSELECT ("DYE_ELV > 20"). The XIS data were selected in 3×3 and 5×5 edit-modes using grades 0, 2, 3, 4, 6. Hot and flickering pixels were removed using the SISCLEAN script.

Spectra were extracted by using circular regions of 2 arcmin radius[4] centred on the NED nuclear position of NGC 4102 (RA (J2000)= 12:06:23.0 and Dec (J2000) = +52:42:40). CXO J120627.3+524303 is reported by the *Chandra* Source Catalogue (CSC) as a source within this extraction region with $F(0.5\text{–}10\ \mathrm{keV}) = 4.8 \times 10^{-14}$ erg s^{-1} cm^{-2}, which is much smaller than that of NGC 4102 (see Table 2).

In addition to NGC 4102, four sources were detected in the XIS field of view: CXO J120543.3+523806, CXO J120548.4+524306, CXO J120600.6+523831, and CXO J120633.2+524022. According to the CSC, these sources have a 0.5–10 keV flux of 7.5, 4.8, 11.0, and 6.7 in units of 10^{-14} erg s^{-1}cm^{-2}. Background spectra were extracted using two circles of 2.5 and 1.7 arcmin radii on the field, excluding the four sources mentioned above and chip corners to avoid the calibration lamps. The response matrix RMF and ancillary response ARF files were created using the tasks XISRMFGEN and XISSIMARFGEN, respectively. Spectra from the two front-illuminated XIS 0 and XIS 3 chips were combined to create a single source spectrum (ADDASCASPEC task), while data from the back-illuminated XIS 1 chip were kept separate. Both resulting spectra were then binned with a minimum of 20 counts in each energy bin in to allow the use of χ^2 statistics using the GRPPHA task.

Suzaku HXD/PIN is a non-imaging instrument with a 34′ square (FWHM) field of view. We reprocessed the HXD/PIN files using standard screening within XSELECT ("T_SAA_HXD > 500" and "COR > 8"). We extracted the spectra and corrected them for dead-time intervals. We used the variable non-X-ray background (NXB) model D (or tuned background, see Fukazawa et al. 2009) that the HXD instrument team provides to correct for particle or detector background. This NXB was added to the cosmic X-ray background (CXB) to produce the final background spectrum. The source was not detected by HXD (see Sect. 3.1.2).

2.2. Chandra data

Level 2 event data from the ACIS instrument were extracted from *Chandra*'s archive[5] (ObsID 4014). The source was observed on 2003 April 3 as part of a snapshot survey of LINERs by Dudik et al. (2005). The data were reduced with the CIAO 3.4[6] data analysis system and the *Chandra* Calibration Database

---

[1] This catalogue included all the nuclei classified as LINERs in the literature to date.

[2] *Suzaku* data has been obtained centring the source on the nominal position of HXD to maximise the S/N.

[3] http://heasarc.gsfc.nasa.gov/docs/suzaku/analysis/abc/

[4] This includes ~90% of the emission of the source.

[5] http://cda.harvard.edu/chaser/

[6] http://asc.harvard.edu/ciao

(caldb 3.4.0). The observation was processed to exclude background flares, using the task lc_clean.sl in source-free sky regions of the same observation. The net exposure time after flare removal is 4.9 ks, and the net count rate in the 0.5–10 keV band is $(6.8 \pm 0.3) \times 10^{-2}$ counts s^{-1}.

The source spectrum was extracted from a circular region with 5 arcsec radius centred on the same position as the extraction used for *Suzaku*/XIS data. The background spectrum was extracted also using a circular region of 18 arcsec centred on RA (J2000) = 12:06:20.7 and Dec (J2000) = +52:42:13. The net number of counts of the spectrum is 340 counts in the 0.5 to 10 keV band. Response and ancillary response files were created using the CIAO mkacisrmf and mkwarf tools. The spectrum was binned to give a minimum of 20 counts per bin.

2.3. Swift/BAT data

The Swift/BAT reduced spectrum was kindly provided to us by the Swift team. It has been derived from an all-sky mosaic in high-energy bins, averaged over 22 months of data, from 2004 December 15 to 2006 October 27, and extracted from a 17 arcmin circular extraction region (see Winter et al. 2008; Tueller et al. 2010, for a detailed explanation of the data processing). NGC 4102 is reported in the 22 months catalogue as one of the 461 sources detected above a 4.8σ level in the 14–196 keV band with BAT (Tueller et al. 2010). It has been detected at the 6.96σ confidence level, and has an average flux of $F(14–196\ \mathrm{keV}) \sim 2.2 \times 10^{-11}$ erg cm^{-2}s^{-1}.

3. X-ray spectral fitting of NGC 4102

In this section we present the results from various model fits to the *Suzaku*, *Chandra*, and Swift data. All the spectral analysis was done using version 12.5.0 of XSPEC. All spectral fits include neutral Galactic absorption ($N_\mathrm{H}(\mathrm{Gal}) = 1.68 \times 10^{20}$ cm^{-2}; Dickey & Lockman 1990). Spectral parameter errors were computed at the 90% confidence level.

3.1. Suzaku spectra

3.1.1. XIS spectra

NGC 4102 is detected with the XIS instrument. The spectral range of 0.6–9 keV for back-illuminated detectors and 0.7–9 keV for front-illuminated detectors were used for the spectral fit of the XIS data. We excluded energies below 0.6 or 0.7 keV (for back- or front-illuminated respectively), between 1.7–1.9 keV, and above 9 keV because of unsolved calibration uncertainties at these energies and low statistics.

There are 4600 net counts in the front-illuminated detectors and 2800 in the back ones. To constrain the shape of the intrinsic continuum, we used the rest-frame 2–6 keV band where we did not expect contamination from other components usually found in the X-ray spectra of AGN (e.g. soft excess emission below ~2 keV and the FeKα emission line at 6.4 keV) and fitted the data to a power-law model. The fit is good (χ^2/d.o.f. = 129.4/114), and the best fit spectral index is $\Gamma = 1.9 \pm 0.2$. Figure 1 shows the ratio between the 0.6–9 keV data and this model (fit statistics of χ^2/d.o.f. = 1332/382). The residual plot indicates excess emission below 2 keV and around the 6–7 keV band.

The FeKα line: the excess emission around 6–7 keV is consistent with the most prominent feature typically observed in the 2–10 keV rest-frame spectra of AGN, i.e. the FeKα emission
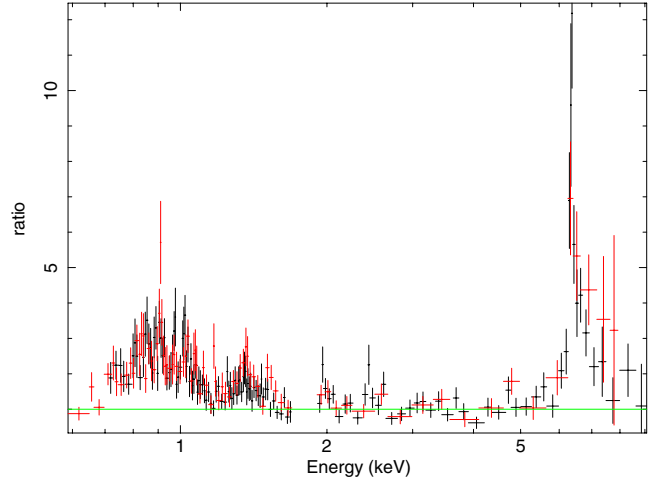
Fig. 1. Ratio between XIS/*Suzaku* data and a power-law model fitted to the 2–6 keV band. Black (dark) points indicate the XIS-0+3 spectrum and red (light) points the XIS-1 spectrum.

Table 1. Results from spectral fitting of the XIS/*Suzaku* data.

Model	A	B	C
	(Models to the 2–9 keV band)		
Γ	$1.6^{+0.1}_{-0.1}$	$1.7^{+0.1}_{-0.1}$	$2.3^{+0.3}_{-0.3}$
$EW(\mathrm{FeK}\alpha)^{(1)}$	$1.3^{+0.2}_{-0.2}$	$0.76^{+0.2}_{-0.2}$	$0.68^{+0.11}_{-0.13}$
$EW(\mathrm{Fe}_\mathrm{XXV})^{(1)}$	...	$0.18^{+0.07}_{-0.07}$	$0.16^{+0.06}_{-0.06}$
χ^2/d.o.f.	214.5/164	188/163	181.7/162
Model	D	E	
	(Models to the 0.6–9 keV band)		
$N_\mathrm{H}^{(2)}$	...	$0.7^{+0.5}_{-0.5}$	
Γ	2.3^*	2.3^*	
$kT^{(3)}$	$0.78^{+0.03}_{-0.03}$	$0.73^{+0.03}_{-0.03}$	
$EW(\mathrm{FeK}\alpha)^{(1)}$	0.68^*	0.68^*	
$EW(\mathrm{Fe}_\mathrm{XXV})^{(1)}$	0.16^*	0.16^*	
χ^2/d.o.f.	456.8/379	445/378	
	Models		
A: *phabs(powerlaw+zgauss)*			
B: *phabs(powerlaw+zgauss+zgauss)*			
C: *phabs(*pexrav*+powerlaw+zgauss+zgauss)*			
D: *phabs(*apec*+*pexrav*+powerlaw+zgauss+zgauss)*			
E: *phabs*(zwabs(*apec*+powerlaw)+*pexrav*+ zgauss+zgauss)*			

Notes. $^{(1)}$ *EW* of emission lines in keV. $^{(2)}$ Intrinsic cold absorber column density N_H in units of 10^{21} cm^{-2}. $^{(3)}$ Temperature of the thermal component kT and *EW*s of the emission lines expressed in keV. * Fixed parameters to the values obtained in *Model C*. See text for details.

line at 6.4 keV. We therefore refitted the 2–9 keV band data with a power law plus Gaussian line model (*Model A* hereafter). The width of the Gaussian was fixed to 0.01 keV (i.e. it was assumed to be intrinsically narrow) and the line centroid energy was fixed to 6.4 keV. Best-fit parameters are listed in Table 1, and the best-fit model, together with the residuals (in the 5.5–7.5 keV range for plotting purposes), is shown in Fig. 2 (left).

We also tested the possibility that the line is broad, by letting the width of the Gaussian profile vary. The best-fit width was $\sigma(\mathrm{FeK}\alpha) = 130^{+70}_{-40}$ eV, but the improvement of the fit was marginal ($\Delta\chi^2 = 3.7$ for one extra parameter, F-statistics probability of 0.09).
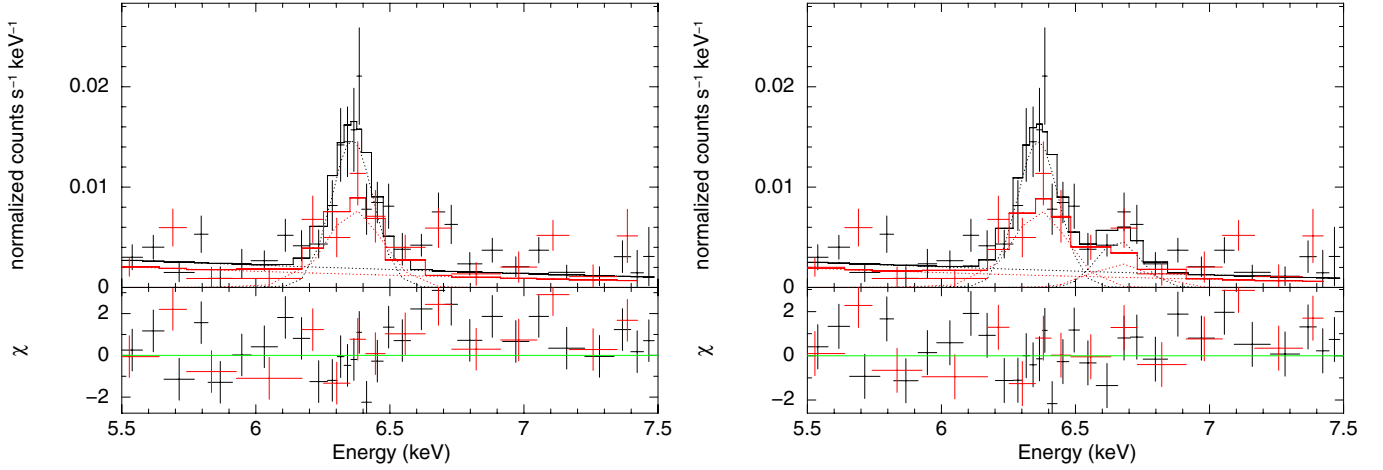
Fig. 2. Best-fit (*top panels*) and residual (*bottom panels*) plots of *Suzaku*/XIS data for *Model A* (*left*) and *Model B* (*right*) around the Fe emission region (black and red points as in Fig. 1). The dotted lines indicate the various model components.
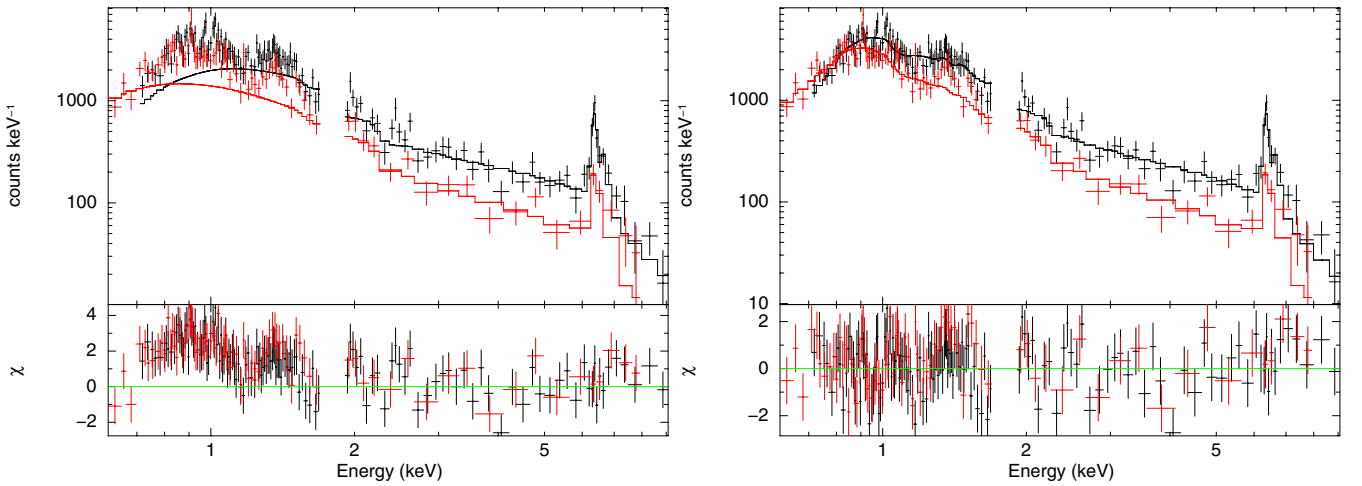
Fig. 3. (*Left*): Extrapolation of the 2–9 keV XIS/*Suzaku* best-fit model (*Model C*) to lower energies. (*Right*): Final fit (*top panel*) and residuals (*bottom panel*) to the XIS/*Suzaku* data using *Model E*. See Table 1 and text for an explanation on the components used in each model.

However, *Model A* is not good enough ($\chi_r^2 = 1.31$). This is mainly because of an emission-line feature at ~6.7 keV (see residuals plot in the left panel of Fig. 2). We therefore included a second Gaussian (which corresponds to the Kα line from Fe$_{XXV}$) to the models with the line energy fixed at 6.7 keV and the width at 0.01 keV (*Model B* hereafter). The fit is significantly improved ($\Delta\chi^2 = 26$, for one extra parameter when compared to *Model A*). The best-fit model is shown in Fig. 2 (right panel) and the best-fit parameter values are listed in Table 1. The power-law index is consistent with the previous value. We also tested the possibility of this line being broad by letting its width be a free parameter. We get a considerable improvement on the fit ($\Delta\chi^2 = 13.5$ for one extra parameter, F-statistics probability of 6.5×10^{-4}) with $\sigma(\text{Fe}_{XXV}) = 390^{+450}_{-105}$ eV. The neutral FeKα line in this case is still consistent with being narrow [$\sigma(\text{FeK}\alpha) < 70$ eV].

The continuum shape in the 2–9 keV band: even after including the 6.7 keV lines the EW of the 6.4 keV line is ~680 eV, which strongly suggests a *Compton*-thick source (see Maiolino et al. 1998). In this case, we expect the presence of a strong reflection component as well. For that reason, we refitted the 2–9 keV spectrum with a model consisting of the two narrow lines at 6.4 keV and 6.7 keV, a power law, and PEXRAV in XSPEC, which describes reflection from neutral material (Magdziarz & Zdziarski 1995). The inclination angle of the reflector was set

to 60° and the iron abundance fixed to 1. PEXRAV was used in such a way that it produces the reflected photons only to test that the spectrum is consistent with a "pure" reflection model. The fit is now acceptable (*Model C* hereafter, see Table 1), and the best-fit spectral index is $\Gamma = 2.3 \pm 0.3$, similar to what is observed in other LINERs (González-Martín et al. 2009a). Finally, we allowed the centroids of the Gaussians to vary. The results do not change and show centroids at $E(\text{FeK}\alpha) = 6.40 \pm 0.02$ keV and $E(\text{Fe}_{XXV}) = 6.73 \pm 0.04$ keV, consistent with the theoretical energies of these transitions. We also tested the width of the lines. The width of the 6.4 keV line is still consistent with zero [$\sigma(\text{FeK}\alpha) < 60$ eV], while the 6.7 keV line is now also consistent with zero $\sigma(\text{Fe}_{XXV}) < 860$ eV.

The full energy band spectrum: our best-fit *Model C* fails to describe the full band well *Suzaku* data (see Fig. 3, left). The spectra show an excess below 2 keV. Many LINERs show a soft excess that can be fitted with a thermal model (González-Martín et al. 2009a; González-Martín et al. 2006). Thus, we added a thermal component (APEC on XSPEC) to the model (*Model D* hereafter). Abundances were fixed to the solar value. The spectral index and the spectral parameter of the reflection component and of the Gaussian lines were kept fixed to those in *Model C*. Best-fit results are listed in Table 1. However, the fit overestimates the spectra below 0.7 keV. To account for
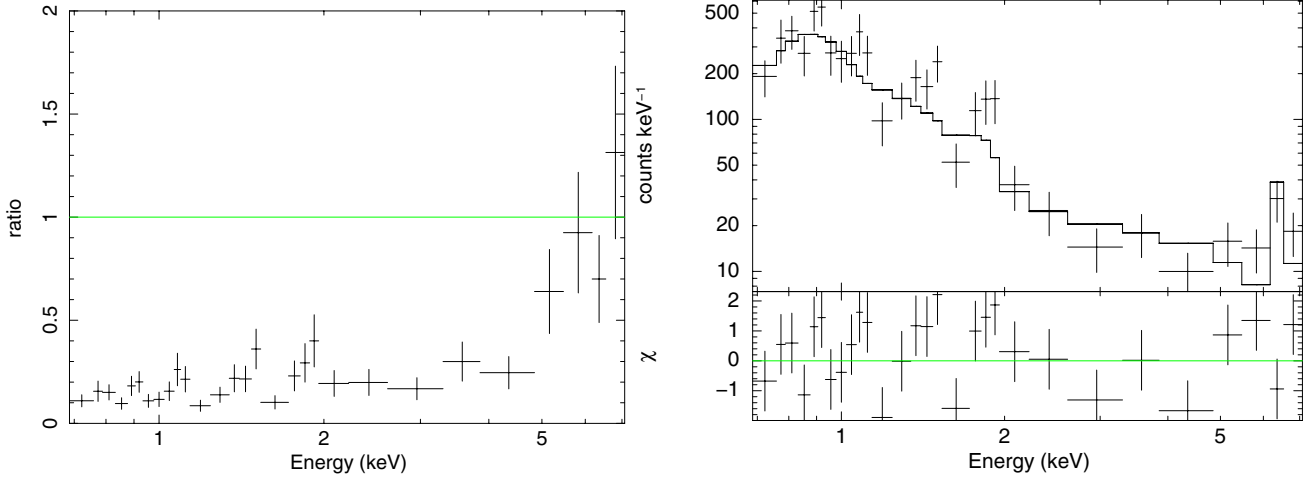
Fig. 4. (*Left*): ratio between the ACIS/*Chandra* and the XIS/*Suzaku* data best-fit *Model E*. (*Right*): *Chandra* best-fit (*top panel*) and residuals (*bottom panel*) using *Model E* and varying the normalisation of the power law and the thermal components by the same amount.

Table 2. Observed fluxes and intrinsic luminosities during the *Suzaku* and *Chandra* observations.

Band	Flux		Luminosity	
(keV)	*Suzaku*	*Chandra*	*Suzaku*	*Chandra*
0.5–2	11.4 ± 0.5	1.6 ± 0.2	10.7 ± 0.9	1.4 ± 0.2
2–10	13.0 ± 0.5	6.1 ± 1.3	8.8 ± 0.8	4.1 ± 0.4
0.5–6	18.1 ± 0.7	3.6 ± 0.4	14.5 ± 0.6	2.9 ± 0.3
6–9	5.0 ± 0.3	4.0 ± 1.5	3.4 ± 0.2	2.1 ± 0.5

Notes. Observed fluxes expressed in units of 10^{-13} erg s^{-1}cm^{-2} and intrinsic luminosities in units of 10^{40} erg s^{-1}.

this, an additional absorber (zwabs in XSPEC) was included, absorbing power-law and thermal components. This model properly describes the XIS/*Suzaku* dataset (*Model E* hereafter, see Table 1 and Fig. 3, right). The best-fit results and the quality of the fit do not differ if we let free the normalisation of the Gaussians and the spectral index: $EW(\text{FeK}\alpha) = 700 \pm 130$ eV, $EW(\text{Fe}_{\text{XXV}}) = 170 \pm 60$ eV, and $\Gamma = 2.4 \pm 0.4$. The resulting temperature and hydrogen column density N_H are consistent with those in other LINERs (González-Martín et al. 2009a). Some residuals still appear in the 1–2 keV band (Fig. 3, right bottom panel). See Sect. 5.4 for a detailed discussion of the soft excess.

The observed fluxes and absorption-corrected luminosities using *Model E* are reported in Table 2. Sixty per cent of the 0.5–2.0 keV flux is contributed by the power law, 38% by the thermal component, and 2% by the reflection component. In the hard band (2–10 keV), 54% of the flux is contributed by the power-law component, while the reflection component, the emission lines, and the thermal component contribute 27%, 17%, and 2%, respectively. The flux of the FeKα line using the *Model E* best-fit results is $F(\text{FeK}\alpha) = 1.5^{+0.3}_{-0.2} \times 10^{-13}$ erg s^{-1}cm^{-2}.

3.1.2. HXD/PIN spectrum

NGC 4102 is not detected by the HXD/PIN above the total background. The count rate of the source is $(4.6 \pm 2.5) \times 10^{-3}$ counts/s, only 1% above the background. We have estimated an upper limit for the source flux of $F(14$–70 keV$) < 1.4 \times 10^{-11}$ erg s^{-1} cm^{-2}, from the accuracy of the NXB model. The expected flux extrapolating *Model E* is

$F(14$–70 keV$) = (1.6 \pm 0.3) \times 10^{-12}$ erg s^{-1}cm^{-2}, consistent with this limit.

3.2. Chandra spectrum

Since the *Chandra* spectrum is part of a snapshot survey, its quality is poorer than the *Suzaku*/XIS spectra. Thus, we decided to fit the *Chandra* spectrum using *Model E* as a baseline. Figure 4 (left) shows the ratio (*Chandra* data)/(*Suzaku* best-fit *Model E*). The source flux was significantly smaller during the *Chandra* observation.

We use different extraction regions for *Chandra*/ACIS and *Suzaku*/XIS (5 arcsec and 2 arcmin, respectively). Thus, this differences could be due to aperture effects. To test this possibility, we re-extracted the *Chandra*/ACIS spectrum using the same extraction region as is used in *Suzaku*/XIS data. The final spectrum is of poorer quality, as expected, so for the spectral fit we used the same model described for the *Chandra* small aperture data (see below) to obtain flux estimates: $F(0.5$–2 keV$) = 3.3 \pm 0.3 \times 10^{-13}$ erg cm^{-2} s^{-1} and $F(2$–10 keV$) = 7.1 \pm 0.7 \times 10^{-13}$ erg cm^{-2} s^{-1}. These fluxes are still well below the *Suzaku* fluxes. Thus, it is unlikely that this variation is due to aperture effects.

This flux deficit could be caused either by an increase in the absorption, or a decrease in the continuum flux. We tested the former by fitting *Model E* to the *Chandra* spectrum, keeping all the model parameters fixed to the values listed in Table 1, apart from N_H. The best-fit model was unacceptable (χ^2/d.o.f. = 221.9/28). We also tested the addition of cold absorption only to the power-law component, but it cannot reproduce the variations (χ^2/d.o.f. = 1483/28) since the flux of the thermal component obtained by *Suzaku* data is well above the *Chandra* 0.5–2.0 keV flux. Thus, cold absorption changes alone do not explain the observed variations. To test the flux variations, we left the normalisations free for the power-law and/or thermal components. Changes of either the power-law component normalisation or the thermal component normalisation alone could not explain the observed variability (χ^2/d.o.f. = 1487/28 and χ^2/d.o.f. = 2942/28, respectively).

Model E fits well the *Chandra* spectrum if we let free the normalisation of both components (χ^2/d.o.f. = 40.7/27). The *Chandra* normalisation of the power-law and thermal components are 12^{+3}_{-2}% and 13^{+6}_{-3}% of the *Suzaku* values, respectively.

The variations are consistent with being the same for both components. In fact, a satisfactory fit is also obtained if we force the same factor of variations in both components (χ^2/d.o.f. = 40.7/28). In this case, the *Chandra* data require both a power-law and thermal component normalisations, which are 12^{+2}_{-1}% of that obtained using *Suzaku* data. This best-fit model is shown in Fig. 4 (right).

Changes in the spectral index and/or other parameter(s) cannot be tested owing the low statistics of the current *Chandra* data set. Nevertheless, we tested the strength of the FeKα emission line by letting the normalisation of the Gaussian component be free. The flux of the FeKα line is $F(\text{FeK}\alpha) = 1.1^{+0.8}_{-0.4} \times 10^{-13}$ erg s^{-1}cm^{-2} (χ^2/d.o.f. = 39.4/27, see Sect. 3.1.1), consistent with the flux of the line inferred from the *Suzaku*/XIS data.

Observed fluxes and intrinsic luminosities for the 0.5–2.0 keV, 2–10 keV, 0.5–6 keV, and 6–9 keV bands are reported in Table 2. While the 6-9 keV band flux is consistent with *Suzaku* observations, the 0.5–6 keV flux is 5 times lower during *Chandra* observation.

3.3. Swift spectrum

The extrapolation of the best-fit *Model E* to higher energies predicts a flux in the 14–70 keV band of $F(14–70 \text{ keV}) \sim 2.1 \times 10^{-12}$ erg s^{-1} cm^{-2}. This is roughly 10% of the Swift/BAT flux, according to the 22 month catalogue of sources (Tueller et al. 2010). Thus, a reflection component alone cannot explain the observed Swift/BAT spectrum.

Since the aperture of *Suzaku*/XIS is smaller than that of Swift/BAT (2 and 17 arcmin, respectively), this discrepancy could come from the difference on the apertures. In addition to NGC 4102, four sources in the XIS field of view may also contribute to the total Swift/BAT flux (namely CXO J120543.3+523806, CXO J120548.4+524306, CXO J120600.6+523831, and CXO J120633.2+524022). According to the *Chandra* Source Catalogue (CSC) these sources have 0.5–10 keV band fluxes of 7.5, 4.8, 11.0, and 6.7 $\times 10^{-14}$ erg s^{-1}cm^{-2}. Their total flux, 2.9 $\times 10^{-13}$ erg s^{-1}cm^{-2}, represents a contribution of 10% to the flux derived for NGC 4102. We extracted the *Suzaku*/XIS spectra of these sources following the same procedure as for NGC 4102. We did not find any indication of reflection-dominated spectra (no hints of the FeKα emission line and the best-fit spectral index is $\Gamma \sim 1.6$–2.0). Even if we assume the worst case scenario in which all the sources contribute above 10 keV with a spectra like NGC 4102, the expected flux cannot explain the excess observed by Swift.

We therefore added a power-law component and absorption to *Model E*, and refitted the Swift/BAT data. Initially, the spectral index of the new power-law component was fixed to the one obtained for *Model E*. The best-fit is acceptable (χ^2_r/d.o.f. = 5.94/6). The best-fit absorption value is $N_H = (2.1^{+2.3}_{-1.9}) \times 10^{24}$ cm^{-2}. If we let the spectral index go free, the best-fit values agree with the previously derived values although with larger uncertainties: $\Gamma = 2.7 \pm 0.8$ and $N_H = (3.9^{+4.4}_{-3.6}) \times 10^{24}$ cm^{-2}. The power-law component is contributing with a flux of $F(14–70 \text{ keV}) = (1.5 \pm 0.4) \times 10^{-11}$ erg s^{-1} cm^{-2}, around ~7 times higher than the reflection component. At the distance of NGC 4102, this implies an intrinsic luminosity of $L(2–10 \text{ keV}) = 1.4 \times 10^{42}$ erg s^{-1}. This value is consistent with the *Suzaku*/HXD flux limit. Figure 5 shows the *Suzaku*/XIS (black
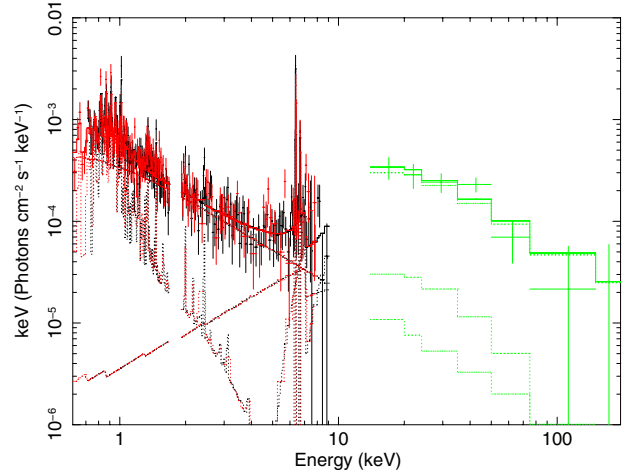
Fig. 5. Best fit to the *Suzaku*/XIS (red and black) and Swift/BAT (green) spectra.

and red points below 10 keV) together with the Swift/BAT (green points above 10 keV), data and best-fit models.

4. Optical and near-IR spectra of NGC 4102

Here we present the optical (TWIN) and near-infrared (LIRIS) spectra contemporaneous with the X-ray *Suzaku* observation. We are only interested in detecting of AGN signatures seen in these spectra, while a more detailed study is beyond the scope of this paper.

4.1. Optical TWIN spectra

Optical spectroscopy was obtained in 2009 July 12 using the TWIN instrument at the 3.5m telescope in Calar-Alto (CAHA[7], Spain). TWIN includes two separate spectroscopic channels ("Blue" and "Red") behind the common entrance slit aperture. Both channels are equipped with a SITe#22b 14 2048 $\times$ 800 CCD detector having a pixel size of 15 microns and a plate scale of 0.56 arcsec pixel^{-1}. Two grating settings were used to cover the optical spectral range: the gratings T8 and T10 provide a wavelength coverage from 3500 to 5600 Å and 5400 to 6700 Å with a dispersion of 1.09 and 0.80 Å pixel^{-1}, respectively. A long slit of 1.2 arcsec width was placed across the galaxy nucleus and oriented at PA = 237° (close to parallactic angle). The average seeing during the observations was ~1.5 arcsec. The slit width was smaller than the seeing in order to avoid any degradation of the spectral resolution. Two exposures of 1200 s were taken for each grating setting. The target spectra were reduced following standard procedures using the spectrum reduction package available in IRAF[8]. For each grating, we built one bias by combining five zero time exposures. After overscan and bias subtraction we divided the image by the normalised flat-field created using a combination of dome flats. Wavelength calibration was obtained using comparison lamp observations done at the same telescope position as that of the target. Flux calibration was performed using two spectrophotometric standard

---
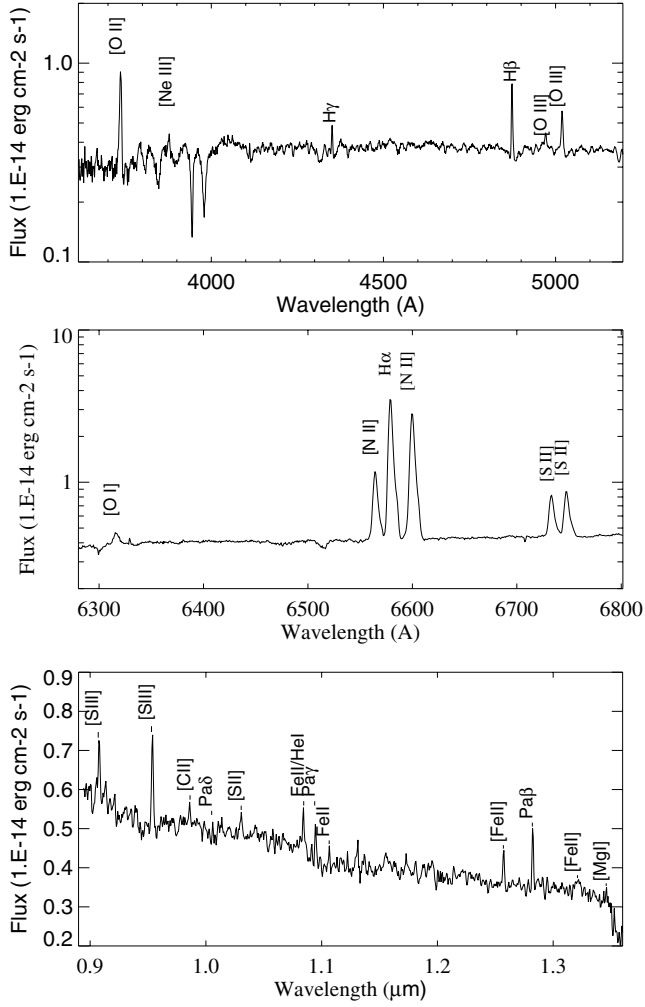
Fig. 6. Optical spectrum observed with TWIN in Calar Alto observatory (*top and middle panels*) and near-infrared spectrum observed with LIRIS in El Roque de los Muchachos Observatory (*bottom panel*). The optical and near-infrared spectra were taken 1 week apart from each other, and one month after the *Suzaku* observation. The optical spectra are in arbitrary units since the absolute calibration could not be done (see text).

Table 3. Optical and near-infrared observed emission lines.

Line	Wavelength (Å)	Flux
[O II] 3727 Å	3736.4 ± 0.11	38.9 ± 1.5
[Ne III] 3869 Å	3876.9 ± 1.01	4.6 ± 1.8
Hγ	4350.9 ± 0.31	5.6 ± 0.9
Hβ	4873.42 ± 0.07	19.3 ± 0.8
[O III] 5007 Å	5019.07 ± 0.18	13.1 ± 0.7
[O I] 6300 Å	6316.34 ± 0.36	3.6 ± 0.4
[N II] 6548 Å	6564.51 ± 0.01	39.0 ± 0.3
Hα	6579.02 ± 0.01	152.9 ± 0.4
[N II] 6584 Å	6600.09 ± 0.01	123.9 ± 0.3
[S II] 6716 Å	6733.25 ± 0.06	21.6 ± 0.3
[S II] 6731 Å	6747.58 ± 0.05	24.1 ± 0.3
[S III] 0.907 μm	9100.5 ± 1.9	24.7 ± 4.5
[S III] 0.953 μm	9562.7 ± 0.5	43.4 ± 3.3
He I 1.087 μm	10871.3 ± 1.2	17.9 ± 2.5
Paγ	10975.5 ± 1.4	13.5 ± 3.3
[Fe II] 1.257 μm	12608.1 ± 0.8	14.2 ± 1.7
Paβ	12859.4 ± 0.9	23.2 ± 3.2

Notes. Observed fluxes expressed in units of 10^{-15} erg s^{-1}cm^{-2}.

The emission-line ratios used to classify the source are

$$\log ([OIII]/H\beta) = -0.17 \pm 0.05, \tag{1}$$

$$\log ([OI]/H\alpha) = -1.63 \pm 0.06, \tag{2}$$

$$\log ([NII]/H\alpha) = -0.091 \pm 0.005 \text{ and} \tag{3}$$

$$\log ([SII]/H\alpha) = -0.524 \pm 0.005. \tag{4}$$

These values are consistent with those reported by Ho et al. (1997) and Moustakas & Kennicutt (2006). This indicates that the source classification remains unchanged regarding its optical spectrum when compared to previous observations. According to the diagnostic diagrams by Kauffmann et al. (2003), NGC 4102 should be classified as a LINER source. We also expect no line flux variation for those species coming from the NLR, along the timeline between the different observations quoted here.

The [O III]λ5007 Å flux, corrected for internal extinction, can be interpreted as an isotropic indicator of the AGN power of the source (Maiolino et al. 1998). In fact, Ganda et al. (2006) show that the [O III] map in NGC 4102 traces the outflowing gas of probably the NLR emission in the AGN. They also show that [O III] emission is extended towards the North-West of the nucleus. We have compared the fluxes of the optical lines in our spectra with those reported in the literature by Ho et al. (1997) and Moustakas & Kennicutt (2006). Some differences are expected from the use of different apertures; thus, while we use an aperture size of 1.2×3.4 arcsec, Moustakas & Kennicutt (2006) and Ho et al. (1997) used an aperture size of 2.5×2.5 arcsec and 2×4 arcsec, respectively. Our fluxes are consistent with those reported by Moustakas & Kennicutt (2006) and ~30% lower than those reported by Ho et al. (1997). Given the flux calibration uncertainties mentioned above, we used our spectra for emission line ratio diagnostics and extinction calculations, but we adopted the better calibrated [O III] flux from Moustakas & Kennicutt (2006)[9]. The calibrated flux from Moustakas & Kennicutt (2006) is $F([O III]) = 1.5 \times 10^{-14}$ erg cm^{-2} s^{-1}. We determined the reddening using the Hα/Hβ and Hβ/Hγ flux ratios and the extinction curve obtained by Calzetti et al. (1994)

stars (BD+28D42118 and Feige11018). The absolute calibration is not accurate enough.

One-dimensional spectra, without sky contribution, were extracted from a 3.4 arcsec aperture centred on the peak of the continuum. They are shown in Fig. 6 (top and middle panels). Recombination lines like Hα, Hβ, and Hγ appear in emission, although an absorption component is also detected. Among the forbidden lines, low-ionisation states dominate ([O I]λ6300 Å, [N II]$\lambda\lambda$6548, 6583 Å, [S II]$\lambda\lambda$6716, 6731 Å, and [O II]λ3727 Å) and intermediate ionisation lines like [O III]λ5007 Å and [Ne III]λ3869 Å are also present. The flux of all lines was measured by fitting a Gaussian profile to each line (see Table 3). In the particular case of the two [N II] and the Hα lines, we de-blended them by modelling the three lines simultaneously, constraining our fit by using the same FWHM for all of them. In the Hβ and Hγ cases, we used two Gaussians to account for the emission and absorption components of these lines. All the lines appear narrow, showing widths below 250 km s^{-1} after deconvolving the instrumental profile. A strong velocity field is seen in the 2-D spectrum at the inner parts of the galaxy, which may produce wings and assymmetries in the line profiles.

---

[9] They used a wide aperture and the slit orientation coincides with the parallactic angle.

to estimate a colour excess of $E(B − V) = 0.99$ (i.e. $Av \sim 3.05$, Cardelli et al. 1989). This colour excess implies a de-reddened [O III]λ5007 Å flux of $F([\text{O III}]) = 3.67 \times 10^{-13}$ erg cm^{-2} s^{-1}. At the distance of NGC 4102, it implies a luminosity of $L([\text{O III}]) = 1.27 \times 10^{40}$ erg s^{-1}.

The X-ray-to-[OIII] ratio, $R_{\text{X/[O III]}}$ can be used as an indicator of the Compton-thickness of the source. The typical limit of a *Compton*-thick source is $R_{\text{X/[O III]}} < 0.5$ (Maiolino et al. 1998; Bassani et al. 1999). The $R_{\text{X/[O III]}} = 0.55^{+0.06}_{-0.07}$ when using *Suzaku* flux measurements, classifying the source as borderline *Compton*-thin source. With the *Chandra* flux, the ratio is $R_{\text{X/[O III]}} = 0.22^{+0.08}_{-0.10}$, corresponding to a *Compton*-thick source.

4.2. Near-infrared LIRIS spectrum

Infrared long slit spectroscopic data in the range 0.9–1.4 μm were obtained in 2009 July 3 with the near-infrared camera/spectrometer LIRIS (Manchado et al. 2004) on the 4.2 m William Herschel Telescope. The LR_ZJ (0.9–1.3 μm) grism was used. We followed an ABBA telescope nodding pattern. The spatial scale is 0.25 arcsec per pixel and the slit width 0.75 arcsec. The total observing time was 3000 s obtained from 5 exposures of 600 s each. The infrared spectrum was taken in order to have a view of the central engine less affected by obscuration with respect to the optical spectrum.

The data were reduced following standard procedures for near-infrared spectroscopy, using the LIRISDR dedicated software developed within the IRAF environment. The basic reduction steps include sky subtraction, flat-fielding, wavelength calibration, and finally the shift-and-add technique to combine individual frames. The nearby star HIP 56334 was observed with the same configuration and similar airmass of the galaxy to perform the telluric correction and flux calibration.

The resulting near-infrared spectrum of NGC 4102, in the 0.9–1.4 μm range extracted from 1 arcsec (4 pixels) aperture is shown in Fig. 6 (bottom panel). Broad permitted lines and coronal lines (e.g. [S IX] and [S VIII]) were not detected. The spectrum is characterised by intense low-ionisation emission lines, consistent with the LINER optical classification of the source. Labels in this figure indicate the securely identified emission lines. The spectrum shows both permitted and forbidden lines. Among the latter, the strongest one are [S III]$\lambda\lambda$ 0.907 and 0.953 μm, although other low-ionisation lines are also present like [S II]$\lambda\lambda$ 1.029 and 1.032 μm, [Fe II]$\lambda\lambda$ 1.257 and 1.321 μm, and [C II]λ 0.982 μm. Among the permitted lines we detect Paβ and Paγ. There is also a hint of Paδ. We also clearly detect a line at 1.087 μm which can be identified as He I and another line centred at 1.095 μm which can be identified as Fe II. The emission lines fluxes were measured using Gaussian fits with an IDL routine (see Table 3).

5. Discussion

We have presented the results from the study of *Chandra*, Swift, and *Suzaku* data of NGC 4102 taken in 2003, 2004–2007, and 2009. The *Suzaku* observations are presented here for the first time. We also present the results from optical (TWIN at Calar Alto observatory) and near-infrared (LIRIS at El Roque observatory) data contemporaneous to the *Suzaku* observations. The summary of the results so far are

– *Suzaku*/XIS spectra of NGC 4102 are better fitted with a model that consists of (i) a power-law with a spectral index of $\Gamma = 2.3$, (ii) a reflection component, (iii) two Gaussian

lines at 6.4 and 6.7 keV, and (iv) a thermal component (we used the APEC model in XSPEC). The broad band spectra are also modified by a cold absorber material with $N_{\text{H}} \sim 1 \times 10^{21}$ cm^{-2}. This is the so-called *Model E* in Table 1 (see also Sect. 3.1).

– The high Fe$K\alpha$ equivalent width [$EW(\text{Fe}K\alpha) = 680^{+110}_{-130}$ eV] strongly supports the *Compton*-thick nature of this source. The Fe$K\alpha$ emission line is also detected in the *Chandra* spectrum with the same flux. We also detected an ionised Fe$_{\text{XXV}}$ emission line at 6.7 keV with an *EW* of $EW(\text{Fe}_{\text{XXV}}) = 160^{+60}_{-60}$ eV.

– No emission above 10 keV is detected with *Suzaku*/HXD, but it is detected with Swift/BAT. The latter is fitted with a combination of power-law component and reflection component (as that used in *Suzaku*/XIS data), plus an additional absorption of $N_{\text{H}} \sim 2 \times 10^{24}$ cm^{-2}. Therefore, the Swift/BAT spectrum offers the first direct look to the intrinsic power-law continuum of this source, which cannot be observed at lower energies because of the large absorption.

– The observed flux below 6 keV in the *Suzaku* data is higher than the *Chandra* flux in the same band. This variation is described better as a decrease in the normalisation of the power-law component *and* the thermal component by a factor of ~7.

– The optical and near-infrared spectra of NGC 4102 show signatures of a classical Type-2 LINER. The source classification remains consistent with previous reported data (Ho et al. 1997; Moustakas & Kennicutt 2006).

– The object, according to the $R_{\text{X/[O III]}}$ ratio is *Compton*-thick during the *Chandra* bservation and border-line *Compton*-thin during the *Suzaku* observation.

In the following sections we discuss the nature of NGC 4102 according to the present results.

5.1. The neutral iron line emission and the Compton-thick nature of the source

The strength of the neutral iron line is quite large, ruling out the hypothesis that it originates in transmission-dominated material. Another possibility is that the line comes from reprocessing from cold, *Compton*-thick matter. Since the observed line is narrow, this material cannot be associated with the inner region of the accretion disc. Moreover, the line flux appears to be constant during the *Chandra* and *Suzaku* observations[10]. This implies that it has to be produced at a distance larger than 2 pc from the central source. Using the relation between the X-ray luminosity and the size of the BLR derived by Kaspi et al. (2005), we inferred a size of the BLR of the source of 1 day-light (~0.001 pc). This distance implies that the iron line is formed in the geometrically thick torus rather than the outer regions of the accretion disc or the BLR.

In this case, the line's high EW rules out inclination angles lower than 60°, and, assuming half opening angles of the torus of 30–45 °, its hydrogen column density must be of the order of $N_{\text{H}} \sim 10^{24}$ cm^{-2} (Ghisellini et al. 1994). Interestingly, this column density agrees very well with the one measured with Swift/BAT data ($N_{\text{H}} \sim 2 \times 10^{24}$ cm^{-2}). We therefore believe that the strength of the 6.4 keV line, its lack of flux variation, and the results from the spectral fitting of the Swift/BAT data, provide

---

[10] Although we do not have evidence of variability, it might be possible that the line has changed in shorter periods of time and by chance it is consistent with being the same at the time of *Chandra* and *Suzaku* observations.

strong evidence of a *Compton*-thick torus, at a distance of ~2 pc from the central source, which is blocking our view.

5.2. The ionised Fe_{XXV} emission line

Ionised line emission can be produced by reflection on an ionised accretion disc (e.g. MRK 766, Miller et al. 2006). This is particularly likely for *EW*s higher than 100 eV. However, if NGC 4102 is *Compton*-thick and we have no direct view to the central source at energies below ~10 keV, the line-emitting region must be located at a considerable distance from the nucleus to be visible. Another possibility is that the line is produced by *Compton*-thin gas that is photoionised by the nucleus. This material could also be responsible for the scattered power-law component seen in the *Suzaku*/XIS energy band. In this case, the *EW* is expected to be lower than ~100 eV (Bianchi et al. 2009). Our measurement of the *EW* is still consistent, within the error bars, with this possibility.

5.3. Absorbers along the line-of-sight

Apart from the *Compton*-thick absorber at ~2 pc away from the central source, the analysis of the *Suzaku*/XIS spectra suggested the presence of a second, *Compton*-thin absorber with $N_H \sim 10^{21}$ cm^{-2}.

In addition, the optical spectrum analysis yielded a reddening of $Av \sim 3.05$. Assuming a Galactic ratio between gas and dust, we used the relation of Bohlin et al. (1978) (i.e., $N_H = 2.2 \times Av \times 10^{21}$ cm^{-2}) to predict a column density of $N_H \sim 6.7 \times 10^{21}$ cm^{-2}, with an uncertainty of ~30%. This value is not consistent with any of the column density estimates of the two X-ray absorbers.

Therefore, it is likely that, apart from the torus blocking the view of the central source, the narrow line region (NLR) and the soft X-ray emitting region are also affected by neutral absorbers, albeit of different column densities. This difference argues against the possibility that these two regions coincide (see also the discussion in the following section). Moreover, they should be located at distances larger than the torus since it is blocking our line of sight. This argues in favour of this material being located far away from the source. Most probably, these two absorbers are associated with the interstellar medium of the host galaxy. This agrees with *HST* imaging observations of this source[11], which reveal a large amount of dust in the central region of this galaxy (see also Beck et al. 2010).

5.4. The puzzling soft X-ray emission in NGC 4102

The "soft excess" seen in the *Suzaku* spectrum is described well by a thermal model with $kT \sim 0.7$ keV. This temperature is consistent with that of thermal component in LINERs (González-Martín et al. 2009a). This thermal component is believed to be associated with extended star-forming regions close to the centre of the host galaxy (Jogee et al. 2005). Another possibility is that the soft X-ray emitting material is located in the NLR of the source photonionised by the central source (e.g. Bianchi et al. 2006; Guainazzi & Bianchi 2007). Ghosh et al. (2008) have used *Chandra* data to study the nuclear morphology of NGC 4102. They detected a "soft" X-rays extended emission, within a radius of 3 arcsec to the west of the nucleus. They suggest that this extended emission could originate in material

photoionised by the AGN at a distance of ~100 pc. This is consistent with the location of the NLR in this object (250 pc), using the relation between the X-ray luminosity and the size of the NLR given by Masegosa et al. (2011).

However, the variability of the soft-excess flux within ~7 years (i.e. between the *Chandra* and *Suzaku* observations) suggests that the material responsible for the soft X-ray emission cannot be associated with the NLR. The difference in the column density of the absorbers "seen" by this material and the NLR, also argues against this possibility. Due to its variability, the soft X-ray emitting region must be located at least within the torus. The material responsible for this emission may also be responsible for the Fe_{XXV} emission line, and the scattering of the nuclear continuum to the line of sight. It is possible that the soft X-ray emission is also nuclear emission, scattered to the line of sight; however, its temperature is significantly higher than the typical temperatures observed in classical AGNs ($kT \sim 0.1$ keV, see e.g. Gierliński & Done 2004).

In any case, it is difficult to understand the origin of the observed variability in soft X-rays and even more the fact that both the power-law continuum and the soft X-ray, "thermal" component vary with a similar factor between the *Chandra* and the *Suzaku* observations. Perhaps the observed variability could be due to a variable source within the *Suzaku* extraction region. As already mentioned in Sect. 2, only one source is seen in *Chandra* image within the *Suzaku* extraction region (CXO J120627.3+524303). This source is located at the end of one of the spiral arms of the host galaxy. The total flux of this source is $F(0.5–10$ keV$) = 4.8 \times 10^{-14}$ erg s^{-1}cm^{-2}, a factor of 40 lower than the power-law plus thermal flux obtained during *Suzaku* observation ($F(0.5–10$ keV$) = 1.8 \times 10^{-12}$ erg s^{-1}cm^{-2}). Although it seems to be an extreme variation, this has already been observed in the case of the Circinus Galaxy, when the high flux state of an extremely variable ultra-luminous X-ray source (ULX) is the most likely explanation for the flux variability of the source (Bianchi et al. 2002). An X-ray monitoring follow up of the source with high spatial resolution, perhaps with *Chandra*, is needed to understand the nature of the "soft-excess" emission and its variability.

5.5. Why NGC 4102 is optically classified as a LINER?

The intrinsic 2–10 keV band luminosity[12] of the source is $L(2–10$ keV$) = 1.4 \times 10^{42}$ erg s^{-1}. It implies a bolometric luminosity of the AGN of $L_{bol} \sim 7 \times 10^{43}$ erg s^{-1}, assuming a bolometric correction of $k_{bol} = 50$ (median value derived for LLAGN, Eracleous et al. 2010). We can also estimate the black hole mass of the source using the correlation found between the black-hole mass and the stellar velocity dispersion by Tremaine et al. (2002). We adopted the stellar velocity dispersion measurements of $\sigma_{bulge} = 174.3$ km s^{-1} (Ho et al. 2009) to estimate a black-hole mass of $M_{BH} = 8 \times 10^7 \, M_\odot$. This estimate is consistent with the average value for LINERs (González-Martín et al. 2009b). Finally, using $\dot{m}_{Edd} = L_{bol}/L_{Edd} = 0.725(L_{bol}/10^{38})/(M_{BH}/M_\odot)$, the derived accretion rate is $\dot{m}_{Edd} = 6 \times 10^{-3}$. This low accretion rate is also common among LINERs.

Moreover, the bolometric luminosity, black-hole mass, and accretion rate for this source are consistent with Type-2 Seyferts (see Figs. 6 and 7 in Panessa et al. 2006). However, the optical and near-infrared spectra show low strength of the coronal lines, characteristic of LINERs. Therefore, there is still an important

---

[11] Images taken from the *Hubble Legacy Archive* (HLA), http://hla/stci.edu/hlaview.html

[12] This luminosity is obtained using the Swift spectral fit and it is corrected for absorption.

open question: why is this source optically classified as a LINER and not as a Type-2 Seyfert?

If we attribute this classification to the absorption, a special configuration of absorbers, partially blocking the continuum emission to reach the NLR has to be claimed. We have demonstrated that NGC 4102 shows a complex structure of absorbers. However, these complex absorbers are also seen in other Type-2 Seyferts and, with the current data, we cannot give any evidence supporting this special location of the absorbers. The difference found between this LINER and Type-2 Seyferts is the steeper spectral index ($\Gamma = 2.3$), which is common in other LINERs (González-Martín et al. 2009a). One possibility is that the continuum emission, i.e. the spectral energy distribution (SED) of this source, and the accretion mode are different than in other AGN.

5.6. The X-ray-to-[O III] ratio as a Compton-thick diagnostic

Finally, we want to make a remark on the implications of the variable X-ray flux detected in this source and the use of $R_{X/[O\ III]}$ ratio as an indicator of Compton-thickness. The [O III] comes from the NLR, which is a rather extended region, therefore its emission is constant. The results of this analysis are consistent with this interpretation, despite the absolute calibration uncertainties. However, this could not be the case for the X-ray flux. The 2–10 keV band flux could vary and affect this ratio. For NGC 4102, the scattering and thermal components change in a factor of 7 between the two observations, strongly affecting also the 2–10 keV flux. These changes can *mimic* a *Compton*-thin source when the source is in a high X-ray flux-state, which it partially does in the case of the *Suzaku* observations for NGC 4102. Therefore, we want to stress that this ratio must be used carefully as a *Compton*-thick indicator.

6. Conclusions

NGC 4102 shows indications of *Compton*-thick material associated to the geometrically thick torus based on the high EW and lack of variability in the neutral iron emission line in the *Suzaku*/XIS data, together with the intrinsic continuum detected with Swift/BAT. Apart from the *Compton*-thick absorber, two more absorbers were derived, from the soft X-rays and the optical spectrum, respectively. They are probably associated with material located in the host galaxy. Moreover, we argued that a material located within the torus and perpendicular to the plane of the disc could be responsible for the observed scattered X-ray continuum component, "soft-excess", and the ionised Fe$_{XXV}$ emission lines. To understand the nature of this material, an X-ray monitoring follow up of the source is required.

Finally, NGC 4102 is consistent with the LINER classification through optical and near-infrared spectra. However, the accretion rate and bolometric luminosity of this source are consistent with other LLAGN like Type-2 Seyferts. We speculate that this classification might be due to a different SED caused by a different accretion mode, based on the steeper spectral index found.

References

Antonucci, R. 1993, ARA&A, 31, 473
Bassani, L., Dadina, M., Maiolino, R., et al. 1999, ApJS, 121, 473
Beck, S. C., Lacy, J. H., & Turner, J. L. 2010, ApJ, 722, 1175
Bianchi, S., Matt, G., Fiore, F., et al. 2002, A&A, 396, 793
Bianchi, S., Guainazzi, M., & Chiaberge, M. 2006, A&A, 448, 499
Bianchi, S., Guainazzi, M., Matt, G., Fonseca Bonilla, N., & Ponti, G. 2009, A&A, 495, 421
Bohlin, R. C., Savage, B. D., & Drake, J. F. 1978, ApJ, 224, 132
Brightman, M., & Nandra, K. 2008, MNRAS, 390, 1241
Calzetti, D., Kinney, A. L., & Storchi-Bergmann, T. 1994, ApJ, 429, 582
Cardelli, J. A., Clayton, G. C., & Mathis, J. S. 1989, ApJ, 345, 245
Carrillo, R., Masegosa, J., Dultzin-Hacyan, D., & Ordoñez, R. 1999, Rev. Mex. Astron. Astrofis., 35, 187
Dewangan, G. C., & Griffiths, R. E. 2005, ApJ, 625, L31
Dickey, J. M., & Lockman, F. J. 1990, ARA&A, 28, 215
Dudik, R. P., Satyapal, S., Gliozzi, M., & Sambruna, R. M. 2005, ApJ, 620, 113
Dudik, R. P., Satyapal, S., & Marcu, D. 2009, ApJ, 691, 1501
Eracleous, M., Hwang, J. A., & Flohic, H. M. L. G. 2010, ApJ, 711, 796
Fabbiano, G. 1989, ARA&A, 27, 87
Fukazawa, Y., Mizuno, T., Watanabe, S., et al. 2009, PASJ, 61, 17
Ganda, K., Falcón-Barroso, J., Peletier, R. F., et al. 2006, MNRAS, 367, 46
Ghisellini, G., Haardt, F., & Matt, G. 1994, MNRAS, 267, 743
Ghosh, H., Mathur, S., Fiore, F., & Ferrarese, L. 2008, ApJ, 687, 216
Gierliński, M., & Done, C. 2004, MNRAS, 349, L7
Gonçalves, A. C., Véron-Cetty, M.-P., & Véron, P. 1999, A&AS, 135, 437
González-Martín, O., Masegosa, J., Márquez, I., Guerrero, M. A., & Dultzin-Hacyan, D. 2006, A&A, 460, 45
González-Martín, O., Masegosa, J., Márquez, I., Guainazzi, M., & Jiménez-Bailón, E. 2009a, A&A, 506, 1107
González-Martín, O., Masegosa, J., Márquez, I., & Guainazzi, M. 2009b, ApJ, 704, 1570
Goulding, A. D., & Alexander, D. M. 2009, MNRAS, 398, 1165
Guainazzi, M., & Bianchi, S. 2007, MNRAS, 374, 1290
Heckman, T. M. 1980, A&A, 87, 152
Ho, L. C. 2009, ApJ, 699, 626
Ho, L. C., Greene, J. E., Filippenko, A. V., & Sargent, W. L. W. 2009, ApJS, 183, 1
Ho, L. C., Filippenko, A. V., & Sargent, W. L. W. 1997, ApJS, 112, 315
Jogee, S., Scoville, N., & Kenney, J. D. P. 2005, ApJ, 630, 837
Kaspi, S., Maoz, D., Netzer, H., et al. 2005, ApJ, 629, 61
Kauffmann, G., Heckman, T. M., Tremonti, C., et al. 2003, MNRAS, 346, 1055
Kinney, A. L., Bohlin, R. C., Calzetti, D., Panagia, N., & Wyse, R. F. G. 1993, ApJS, 86, 5
Magdziarz, P., & Zdziarski, A. A. 1995, MNRAS, 273, 837
Maiolino, R., Salvati, M., Bassani, L., et al. 1998, A&A, 338, 781
Manchado, A., Barreto, M., Acosta-Pulido, J., et al. 2004, Proc. SPIE, 5492, 1094
Masegosa, J., Márquez, I., Ramirez, A., & González-Martín, O. 2011, A&A, 527, A23
Mateos, S., Barcons, X., Carrera, F. J., et al. 2005, A&A, 444, 79
Miller, L., Turner, T. J., Reeves, J. N., et al. 2006, A&A, 453, L13
Mitsuda, K., Kamazaki, T., Saito, M., Yamaguchi, N., & Kohno, K. 2007, PASJ, 59, 1
Moustakas, J., & Kennicutt, R. C., Jr. 2006, ApJS, 164, 81
Panessa, F., & Bassani, L. 2002, A&A, 394, 435
Panessa, F., Bassani, L., Cappi, M., et al. 2006, A&A, 455, 173
Rees, M. J. 1984, ARA&A, 22, 471
Tremaine, S., Gebhardt, K., Bender, R., et al. 2002, ApJ, 574, 740
Tueller, J., Baumgartner, W. H., Markwardt, C. B., et al. 2010, ApJS, 186, 378
Tully, R. B. 1988, Science, 242, 310
Tzanavaris, P., & Georgantopoulos, I. 2007, A&A, 468, 129
Winter, L. M., Mushotzky, R. F., Reynolds, C. S., & Tueller, J. 2009, ApJ, 690, 1322
Winter, L. M., Mushotzky, R. F., Tueller, J., & Markwardt, C. 2008, ApJ, 674, 686